Discrete element modelling of concrete submitted to dynamic loading at high strain rates

Sébastien Hentz, Frédéric Donzé, Laurent Daudeville

Discrete element modelling of concrete submitted to dynamic loading at high strain rates

Sébastien Hentz*, Frédéric V. Donzé, Laurent Daudeville

Laboratoire Sols, Solides, Structures, Domaine Universitaire, B.P. 53, 38041 Grenoble Cedex9, France

The use of a 3D discrete element method (DEM) is proposed to study concrete submitted to dynamic loading. The model has already been validated through quasi-static simulations. This paper aims first at extending the validation of the model and at contributing to the understanding of the physical mechanisms in stake. Once the correct quasi-static identification of the model parameters is done, compressive dynamic tests are first simulated. Unchanged, the model proves able to reproduce the concrete strain rate dependency, and confirms the inertia-based hypothesis at high strain rates. Dynamic tensile tests show that a local rate effect has to be introduced to reproduce the experimental rate dependency, which would then be a material-intrinsic effect.

1. Introduction

Numerous types of structures may be exposed to dynamic loading at a wide range of strain rates (see Fig. 1), which is why the dynamic behaviour of (plain) concrete has been extensively studied. One of the main features of concrete dynamic behaviour, that a model must reproduce, is the significant enhancement of the apparent concrete strength with the strain rate. The understanding of this rate effect has been the purpose of many experimental works, as well as of numerous models.

---
* Corresponding author.

E-mail addresses: sebastien.hentz@inpg.fr (S. Hentz), frederic.donze@hmg.inpg.fr (F.V. Donzé), laurent.daudeville@inpg.fr (L. Daudeville).

1.1. Experimental background

Various experimental devices have been used to explore a wide range of strain rates, as described in [4,19]. Compression and direct tension tests have been performed, from static loading up to strain rates of 10^{-1} s^{-1} with a hydraulic testing machine, whose displacement control capabilities or stiffness are limiting [4]. Charpy Impact tests were commonly used, and significant results are found in the literature, up to 10^{0} s^{-1}. These tests were once mainly qualitative, and advances have been made with instrumented Charpy impact tests [19]. But difficulties remain with the measurement of the data at higher rates. With Drop Weight Impact Tests, rates of 10^{1} s^{-1} may be reached, but the energy transmitted to the specimen is limited by the size of the device: weights around 50–100 kg are dropped from heights of 2–6 m. Higher strain rates in tension and compression, up to more than 10^{2} s^{-1} are obtained

Nomenclature

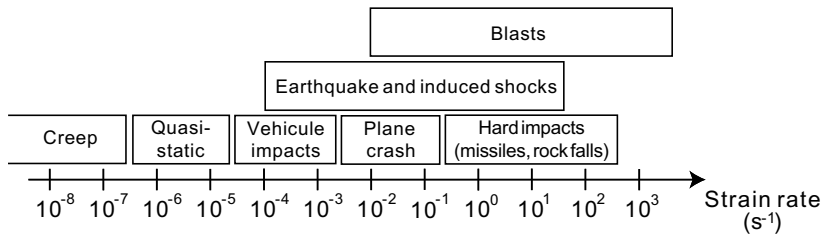|				
c	local cohesion		V_e	ejection velocity of a fragment
C_o	celerity of the specimen's medium		V_{input}	input velocity at the bar–specimen interface
$D^{a,b}$	D distance between centroids of two discrete elements a and b		V_{output}	output velocity at the bar–specimen interface
E	Young's modulus		$\mathbf{x}^a$	$\mathbf{x}$ position vector of a discrete element a
$\mathbf{F}$	interaction force vector		Z_c	distance from the rupture to the free end of the specimen
$\mathbf{F}_n$	normal interaction force vector			
F_n^{max}	maximum normal force		*Greek symbols*	
$\mathbf{F}_s$	shear interaction force vector		β	softening factor
F_s^{max}	maximum shear force		ε_i	strain of the longitudinal incident wave
$\mathbf{F}_s^{reduced}$	updated shear force vector during slip		ε_r	strain of the longitudinal reflected wave
F_{input}	input force at the bar–specimen interface		ε_t	strain of the longitudinal transmitted wave
F_{output}	output force at the bar–specimen interface		$\dot{\varepsilon}_s$	average strain rate imposed on the specimen
G_f	Fracturation energy of the material		$\dot{\varepsilon}$	strain rate
K_n	interaction normal stiffness		$\dot{\varepsilon}_{stat}$	quasi-static strain rate at which the quasi-static properties of the concrete have been identified
K_s	interaction shear stiffness			
l	length of the real specimen			
$\mathbf{n}$	unit interaction vector		γ	interaction range
R_a	R radius of a discrete element a		v	Poisson's ratio
S	cross-sectional area of the real specimen		ϕ_i	internal friction angle
S_{int}	average surface where an interaction is defined		ϕ_c	contact friction angle
T	local maximum tensile strength		ρ	density of the specimen
T_{cs}	local static tensile strength		σ_s	average stress imposed on the specimen
T_{td}	local dynamic tensile strength		σ_c	compressive strength
T_{ts}	local static tensile strength		σ_d	dynamic strength
$\mathbf{U}_n$	normal displacement vector of one element		σ_{cs}	compressive static strength
$\mathbf{U}_s$	tangential displacement vector of one element		σ_t	tensile strength
			σ_{td}	tensile dynamic strength
$\mathbf{V}_a$	velocity vector of the element a		σ_{ts}	tensile static strength

Fig. 1. Regimes of strain rates [4,8].

with a Split Hopkinson Pressure Bar (SHPB) Test which has now become very popular with the introduction of data processing allowing a good precision. Even higher strain rates ($\dot{\varepsilon} \geqslant 10^3$ s^{-1}) may be reached with the use of explosive charges.

The strain rate effect has been studied on different characteristics of concrete: Young's modulus, Poisson's ratio, energy-absorption capacity and axial strain at maximum strength are rate-sensitive quantities, but at a much lower intensity than the compressive and tensile strengths [5,44,45].

Finally, a large part of the results is compiled in Figs. 2 and 3, in terms of the ratio dynamic strength over static strength. Two distinct types of behaviour can be observed: The first one shows a linear dependence of the ratio with log($\dot{\varepsilon}$). The second one is a sharp rise in the rate
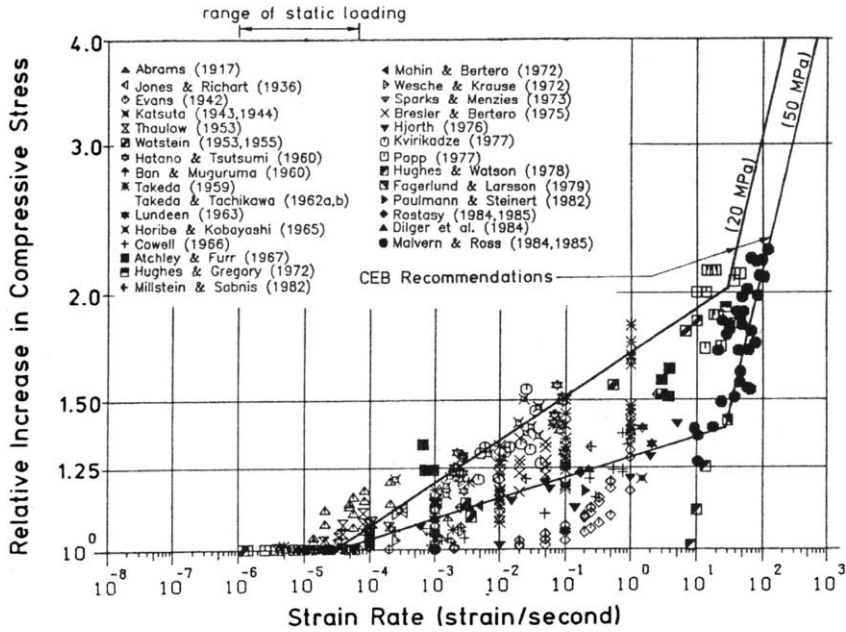
2

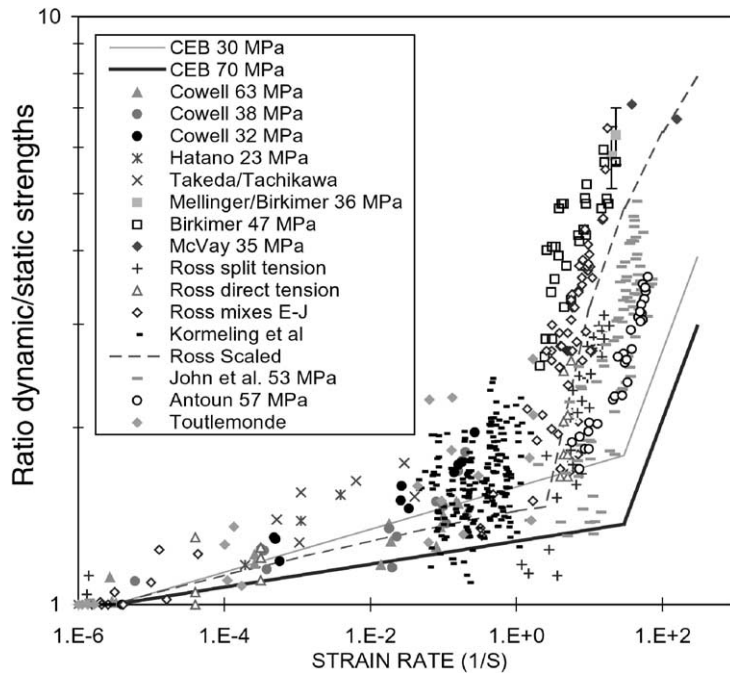Fig. 2. Strain rate dependency of the compressive strength [4].

Fig. 3. Strain rate dependency of the tensile strength [34].

dependence. The limit between the two is around $\dot{\varepsilon} \simeq 3 \times 10^1$ s^{-1} in compression and around $\dot{\varepsilon} \simeq 10^0$ s^{-1} in tension.

To fully understand the rate effect, it is important to be able to answer the following question: is it a material-intrinsic effect, or rather a structural effect, the state of stress and strain not being homogeneous in the specimen? To do so, it is necessary to look at some results concerning the influence of different parameters on this ratio: ratio water/cement $= w/c$ [5,19,45], boundary

3

conditions [4] and presence of free water [42,45]. It first appears that w/c and boundary conditions are secondary parameters, as they have only a slight influence (nevertheless, it seems that the strain dependence is higher for concretes with lower strengths). Moreover, the ratio dynamic strength over static strength seems to be rather more rate-sensitive in tension than in compression. On the other hand, it now seems clear that the strain rate effect at least when $\dot{\varepsilon} \leqslant 10^1 \mathrm{~s}^{-1}$ is explained by the presence of free water in concrete, inducing an effect similar to the Stefan effect [42]. For higher strain rates, the situation is much less clear: in tension, some new insights were recently proposed by Hild et al. [22] and in compression, Janach [25] proposed the hypothesis that the effect of bulking combined with inertia was responsible for the increase of load-carrying capacity of the specimen, making it a structural effect. The aid of powerful models was needed to confirm this hypothesis.

1.2. Modelling background

First of all, the numerous models used to represent concrete-like materials can be classified in three categories, associated with a class of loading [17]: The first one corresponds to a mostly uniaxial loading, where the main physical behaviour is micro-cracking. The second one deals with strong multiaxial loading, where plastic flow occurs. The third one is concerned with high pressure loading, when compaction occurs, and usually strain rate dependency is neglected.

We will ignore the last two classes of model, considering that the stress state of structures submitted to dynamic loading at strain rates of interest here is strongly deviatoric. In this matter, concrete has been extensively modelled, mostly with elasto-plastic models, either with or without associated flow rules. The cracking may be taken into account with smeared cracked models which introduce a loss of rigidity in the direction perpendicular to the direction of maximum tensile stress [43], or damage models [35]. In the dynamic case, models differ in particular in the way strain rate dependency is represented.

Some authors introduce viscosity [4]. Others introduce viscosity combined with inertia, one of the two effects becoming preponderant, depending on the value of the strain rate [17]. Some micromechanics-based fracture models have considered that the crack growth was thermally-activated [19] introducing an activation energy, or a characteristic time of loading [28]. This leads to the following type of dependence: $\sigma_\mathrm{d} \propto \dot{\varepsilon}^n$, where σ_d is the strength. It is also the case of the CEB formulation [1], one of the most comprehensive model, based both on test results and analytical models, and of direct use in numerical analyses. It takes into account most of the experimental observations described in the previous section (see Fig. 2 and 3). This model will be discussed later in this paper.

When it comes to FE computational modelling, attention has to be paid to the fact that the softening behaviour of all these models may cause the loss of objectivity with respect to the mesh in dynamic problems. This may be solved by the use of different regularization techniques, like the crack band model [3], the Cosserat media [6], or the non-local approach [38].

The increasing complexity of these models, associated with the difficulties of dynamic problems, make their computational use somewhat awkward, in terms of either implementation, convergence, or simply cost. In particular, the occurrence of cracking often has to be identified, and effects like internal friction after crack opening, or structural effects like inertia of micro-cracking have to be explicitly accounted for.

1.3. Objectives

This paper proposes the use of the discrete element method (DEM) [12], which is an alternative to continuum-type methods, to study the dynamic behaviour of concrete at high strain rates, where the rate effect is not clearly understood as previously mentioned. This method does not rely upon any assumption about where and how a crack or several cracks occur and propagate, as the medium is naturally discontinuous and is very well adapted to dynamic problems.

Nevertheless, when one uses a DEM model, one has to address the issue of the modelling scale: the DEM is of course particularly adapted to the modelling of granular material [11,24,30], in which case one element represents one grain. Numerous authors have also used the DEM to simulate cohesive geomaterials like concrete, at the scale of the heterogeneity [39,41], that is to say the size of one element is of the order of the biggest heterogeneity, around 1 mm. This approach allows a better understanding of concrete fracture, but of course makes real structures modelling impossible, as the computation cost becomes ''gigantic'' (see [33] with Lattice-type models). Another approach consists in using a higher scale model, which considers that the whole assembly of elements must reproduce the macroscopic behaviour of concrete. Thus some authors like [10,31,36] have modelled impacts on concrete structures, but usually, the model parameters are identified directly on the impact tests, and the different components of the model are not validated through more simple tests.

The purpose of this paper is two-fold: Keeping in mind that the final goal is to represent 3D concrete structures, this work aims at extending the validation of a three-dimensional distinct element (DE) model through the simulation of SHPB tests at high strain rates, and at contributing to the understanding of the physical principles in stake. The DE model has been fully described and validated in quasi-static problems as well as in dynamic compression in [21]. It is to be noted that in the

proposed approach, the local parameters are identified thanks to a quasi-static process, allowing the control of the modelling scale imposed by the available computing power. Firstly, the model and the compression results will be briefly reminded, and then the results of tensile SHPB tests will be presented.

2. DEM model used

It is of importance that the discrete model should be able to reproduce two particular points of the concrete behaviour, with a low computation cost:

1. Sound concrete behaviour is linear, elastic, isotropic and homogeneous.
2. The non-linear behaviour of concrete is more similar to a nearly non-porous medium than to a granular material.

The present numerical model has been implemented within the "Spherical Discrete Element Code" [13]. It uses discrete spherical elements of individual radius and mass, which allows an obvious and quick computation of the contacts. But the orientation distribution of these latter has to be as homogeneous as possible to satisfy the first condition, and the assembly of elements has to be as compact as possible to satisfy the second condition. This is obtained through the use of a particular "disorder" technique (see [14], based on an algorithm described in [26]) which gives a polydisperse assembly with a particular size distribution. Once the assembly has been set, pairs of initially interacting discrete elements are identified. These interactions have been chosen to represent as well and as simply as possible, the elastic and cohesive nature of concrete. To do this, elastic forces with a local rupture criterion are applied between two interacting elements.

Using the constitutive equations for each interaction, the numerical model solves the equations of motion. The explicit time integration of the laws of motion will provide the new displacement and velocity for each discrete element.

As time proceeds during the evolution of the system, change in the packing of discrete elements may occur and new interactions be created. One of the features of this numerical model will then be to determine the interacting neighbours of a given element. This will be achieved by defining an interaction range and identifying all elements within it which are interacting.

2.1. Interaction range

The overall behaviour of a material can be reproduced by means of this model by associating a simple constitutive law to each interaction. An interaction between elements a and b of radius R_a and R_b respectively, is defined within an interaction range γ and does not necessarily imply that two elements are in contact. Then, these elements will interact if,

$$\gamma(R_a + R_b) \geqslant D^{a,b} \tag{1}$$

where $D^{a,b}$ is the distance between the centroids of elements a and b and $\gamma \geqslant 1$. This is an important difference from classical discrete element methods which use spherical elements where only contact interactions are considered ($\gamma = 1$). This choice was made so that the method could simulate materials other than simple granular materials in particular those which involve a matrix as found in concretes. Its principal effect is the increase of the contact number for an equal number of elements, which helps obtaining a homogeneous contact orientation distribution (cf. condition 1). Beside, it increases as well the "effective" size of the elements, which virtually increases the assembly compacity (cf. condition 2), and helps in modelling with a DE model materials which may be considered as continuous at this scale.

2.2. Elastic properties

The interaction force vector $\mathbf{F}$ which represents the action of element a on element b may be decomposed into a normal and a shear vector $\mathbf{F}^n$ and $\mathbf{F}^s$ respectively, which may be classically linked to relative displacements, through normal and tangential stiffnesses, K_n and K_s.

$$\begin{cases} \mathbf{F}_n = K_n \cdot \mathbf{U}_n \\ \Delta\mathbf{F}_s = K_s \cdot \Delta\mathbf{U}_s \end{cases} \tag{2}$$

where U_n is the relative normal displacement between two elements, and ΔU_s is the incremental tangential displacement. The strain energy stored in a given interaction cannot be assumed to be independent of the size of the interacting elements. Therefore interaction stiffnesses are not identical over the sample, but follow a certain distribution, which is another important particularity of the SDEC model. The macroscopic elastic properties, here Poisson's ratio v, and Young's modulus E, are thus considered to be *the input parameters of the model*.

"Macro-micro" relations are then needed to deduce the local stiffnesses from the macroscopic elastic properties and from the size of the interacting elements. Compression tests have been run with one given sample and values linking Poisson's ratio v, and Young's modulus E to the dimensionless values of $\frac{K_s}{K_n}$ were obtained. To fit these values, relations based on the best-fit model [32] are used:

$$\begin{cases} E = \dfrac{D_{\text{init}}^{a,b}}{S_{\text{int}}} K_{\text{n}} \dfrac{\beta + \gamma \frac{K_{\text{s}}}{K_{\text{n}}}}{\alpha + \frac{K_{\text{s}}}{K_{\text{n}}}} \\[3mm] v = \dfrac{1 - \frac{K_{\text{s}}}{K_{\text{n}}}}{\alpha + \frac{K_{\text{s}}}{K_{\text{n}}}} \end{cases} \qquad (3)$$

where $D_{\text{init}}^{a,b}$ is the initial distance between two interacting elements a and b, coefficients α, β and γ are the fitted values and S_{int} is an "interaction surface":

$$S_{\text{int}} = \pi (\min(R_a, R_b))^2 \qquad (4)$$

These relations are simply inverted to obtain the local stiffnesses.

2.3. Inelastic behaviour

2.3.1. Before rupture

To reproduce the behaviour of geomaterials like rocks and concrete, a modified Mohr–Coulomb rupture criterion is used. Thus, for a given interaction, a maximum tensile strength T (with $T > 0$) is given and defines a maximum normal force $F_{\text{n}}^{\max} = -T S_{\text{int}}$ where $F_{\text{n}} = \mathbf{F}_{\text{n}} \cdot \mathbf{n}$, $\mathbf{n}$ being the normal contact unit vector.

The maximum shear force can be calculated as

$$F_{\text{s}}^{\max} = c S_{\text{int}} + F_n \tan \phi_{\text{i}}, \qquad (5)$$

where F_{s} is the absolute value of the shear force, c is the cohesion and ϕ_{i} is the "internal" friction angle. If F_{s} is greater than $F_{\text{s}}^{\max}$, then the shear force is reduced to the limiting value and written as

$$\mathbf{F}_{\text{s}}^{\text{reduced}} = \frac{F_{\text{s}}^{\max}}{F_{\text{s}}} \mathbf{F}_{\text{s}}. \qquad (6)$$

Finally the model is consistent with the behaviour of concrete. Failure comes with the coalescence of microcracks undergoing tension.

2.3.2. After rupture

After initial interactions have broken, new ones are identified, which are not cohesive any more: they are merely "contact" interactions, and cannot undergo any tension force. Then a classical Coulomb criterion is used, with a "contact" friction angle, ϕ_{c}.

Fig. 4 summarizes the rupture criteria used in the model.

It is to be noted that the model is enriched with a local softening factor β, without which the obtained macroscopic behaviour would be somewhat too brittle.

2.4. Parameters calibration

Calibration of the model parameters is necessary to adjust the properties of the material represented by the assembly of discrete elements to the real geomaterial properties, a particular type of concrete. For this purpose, a quasi-static uniaxial compression/traction proce-
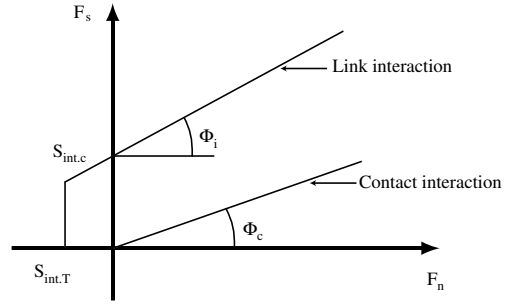

Fig. 4. Rupture criteria used in the model.

dure has been established and is fully described in Hentz et al. [21]. This procedure allows to determine for a single assembly the values of the local parameters T, ϕ_{i}, ϕ_{c}, β and γ to obtain the macroscopic behaviour characterized by the Young's modulus, the Poisson's ratio, the tensile and compressive strengths, as well as the fracture energy. As far as the macroscopic elastic properties are concerned, it appeared that the "macro-micro" relationships discussed in Section 2.2 give only a good approximation of the macroscopic elastic properties, because of the random aspect of the generation of the assembly. To solve this problem, the procedure is the following:

1. A compact, polydisperse discrete element assembly is generated.
2. An elastic compression test is run with elastic local parameters given by the "macro-micro" relations.
3. A correction is applied according to an energy-based criterion, in relation with the characteristic size of the elements.
4. Compressive and tensile rupture axial tests are simulated to deduce the remaining local parameters.

Remark 1. As previously mentioned, spherical elements allow an obvious treatment of the contacts. Nevertheless, this is a rather simplistic way to model the complexity of the microscopic phenomena, and in particular, particle rotations are not well constrained. This is now a well-known problem in the DE modelling of granular materials [15,27,30], and different solutions may be used: less regular shaped elements [41] or the introduction of a law couple/rotation [24]; to obtain a reasonable friction angle, Calvetti et al. [9] simply inhibit the rotations. DE modelling of cohesive materials have been the purpose of much less work, thus the effect of spherical elements was unknown until recently: though less critical, Huang [23], Hentz et al. [20] have shown that it leads to a compressive/tensile strengths ratio too low. Again, this may be solved by the use of less regular shaped elements [40], and by the constraint of the rotations, which has been chosen for the present study (see Hentz et al. [20] for a description).

6

Conclusion. To summarize, the presented approach allows us to control the modelling scale. Its specific and original features are the use of simple ingredients, an interaction range, and an identification process based on quasi-static uniaxial tests. The latter gives the value of the local parameters, and ensures that the quasi-static behaviour of concrete is well reproduced. Thus, in the following computations, no parameter has been identified with the dynamic tests: they are real predictive simulations.

3. Dynamic simulations: the SHPB experiments

3.1. Dynamic compression

A typical SHPB (Split Hopkinson Pressure Bar) experimental setup [46] can be seen in Fig. 5.

It consists of two long aligned metallic bars and a short concrete specimen between them. A projectile impacts the free end of the input bar thus leading to the development of a compressive longitudinal incident wave $\varepsilon_i(t)$. Once it arrives at the bar–specimen interface, it splits into a reflected wave $\varepsilon_r(t)$ which travels in the input bar and a transmitted wave $\varepsilon_t(t)$ which travels in the output bar. These three waves are recorded by gauges which have been cemented on each bar. Data recorded from the gauges have to be shifted to deduce the forces (F_{input} and F_{output}) and velocities (V_{input} and V_{output}) on both faces of the specimen. This processing is highly difficult, as it demands correction techniques to allow very accurate information, which is now possible [18].

Classical SHPB analysis relies on several assumptions:

1. One-dimensional wave propagation theory describes accurately the propagation of waves along the bars.
2. Stress and strain fields in the specimen are uniform in the axial direction.
3. The specimen inertia is negligible.
4. Friction effect in the compression test is negligible.

Data recorded from the gauges have to be shifted to deduce the forces (F_{input} and F_{output}) and velocities (V_{input} and V_{output}) on both faces of the specimen. This processing used to be done according to the first assumption, as the SHPB method was first intended

for metal testing. Metal specimens had a low diameter to avoid radial dispersion in the wave propagation. But concrete testing requires large specimen diameter because of the grain size, which enhances the radial dispersion and demands the use of correction techniques, as proposed by [18], which allows very accurate information on the faces of the specimen.

In addition, metal specimens had a low length, so several wave reflections quickly occurred, satisfying assumption two. In our case, the understanding of brittle failure of concrete demands the investigation of the transient state of the specimen, as well as the structural effects like inertia and friction.

Moreover, Gary and Zhao [18] showed that a so-called three-waves formula gives a correct average strain rate and a correct average stress imposed on the specimen, so that,

$$\dot{\varepsilon}_s(t) = \frac{V_{output}(t) - V_{input}(t)}{l_s} \tag{7}$$

$$\sigma_s(t) = \frac{F_{input}(t) + F_{output}(t)}{2S_s} \tag{8}$$

where l_s and S_s denote respectively the length and the cross-sectional area of the specimen.

3.1.1. The experimental data set

SHPB tests on concrete specimens have been carried out by Gary and Zhao [18], Gary [16]. The data set is shown in Fig. 6.

The concrete specimens that are used are cylinders with a height of 0.036 m and a diameter of 0.036 m. The density is 2500 kg/m³ and the average compressive wave velocity is 3865 m/s [44].

Three loading experiments, ms2b, ms3b and ms5b respectively at 350, 500 and 700 s⁻¹ strain rate have been run and for each of these runs both the input and output velocities and forces are plotted.

3.1.2. Numerical setup

Up to 6200 spherical discrete elements with sizes ranging from 9×10^{-4} to 47×10^{-4} m, have been used to build the numerical concrete sample.

Local parameters were calibrated using the quasi-static procedure already discussed to obtain the expected concrete behaviour: Density 2500 kg/m³, Young's
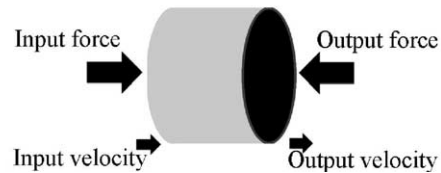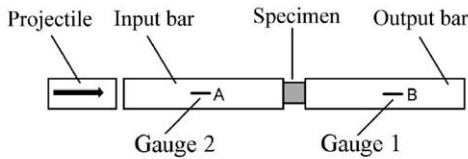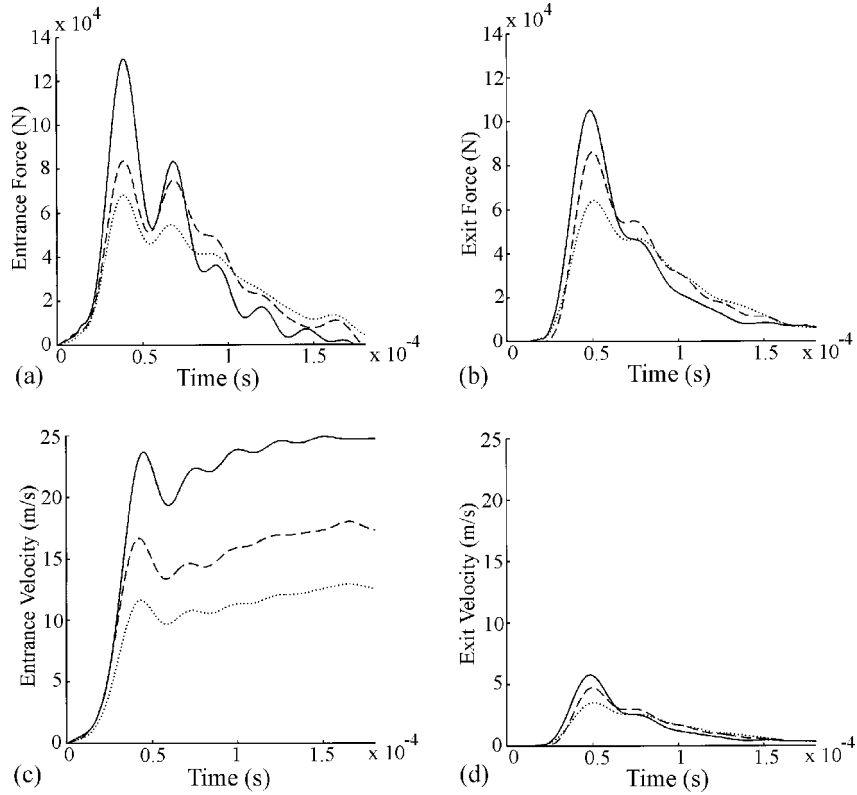

Fig. 5. Setup for SHPB experiment.

Fig. 6. Measured experimental data from compressive SHPB tests. Solid, dashed, and dotted line are, respectively, experiments ms5b, ms3b and ms2b.

modulus 30 GPa, Poisson's coefficient 0.2, compressive strength 60 MPa, and tension strength 5 MPa.

The experimental input and output velocities are applied to the platens. The radial displacement values are assumed to be zero on the input and output surfaces. The resulting input and output forces are computed by summing all the forces applied on the platens. Given the experimental velocity histories, at each time step the applied input and output velocities are updated leading to the computation of numerical force histories, compared with experimental forces.

3.1.3. Results

Fig. 7 shows stress/strain curves obtained for the three tests (Stress and strain are given by the Eqs. (7) and (8)). The experimental curves are very well fitted in the pre-peak region, but this is less often the case after the peak, except for ms2b. Maximum amplitudes of computationed stress fit the experimental stress quite well, despite the recording problems of the tests. Moreover, Fig. 8 shows the damage state of the sample for a given stress of 50 MPa in the elastic phase, for the slowest and the fastest test. As the damage increases, the color darkens. It can clearly be seen that as the strain rate

increases, the extent of the damage lessens. Moreover, this damage, very diffuse, is not homogeneous and tends to propagate inwardly from the lateral free surfaces of the specimen thus forming a contact cone as seen in real experiments.

This result confirms the inertia-based hypothesis first proposed by Brace and Jones [7] and Janach [25]: In this range of strain rates, the rate effect is a consequence of the transition from a state of uniaxial strain into uniaxial stress. This transition is accompanied by bulking, as a result of which the material must accelerate in the radial direction, giving rise to inertial forces. The outer region of the specimen then plays a confining role, preventing the central core from unloading and thus giving the specimen a greater apparent load carrying capacity. Because of the fretting condition on the boundary, the unloading front from the free surface is not parallel to it, explaining the cone-like shape of the damage distribution.

With the 3D DE model, the transient specimen state of damage and stress may be investigated and quite accurately represented, without having to identify a particular cracking zone. What is more, it proves able to quantitatively reproduce the increase of compressive
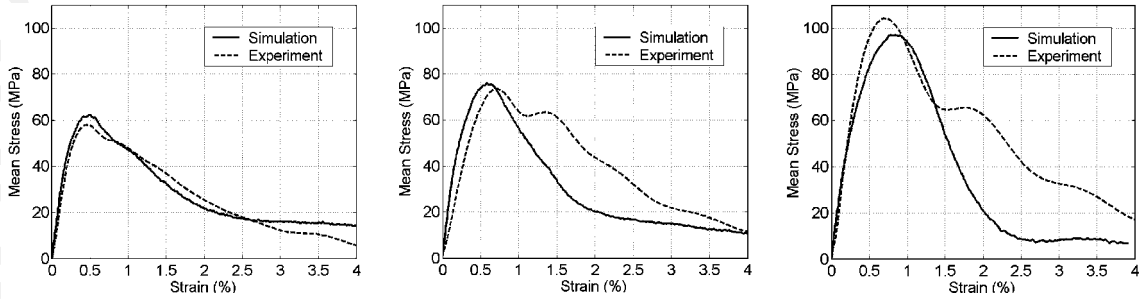
8

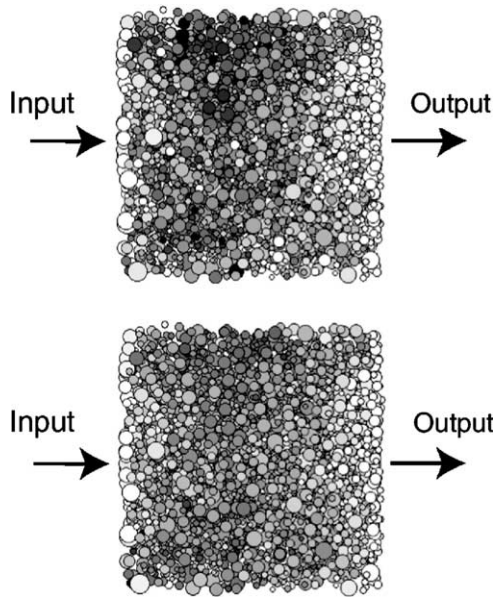Fig. 7. From left to right: Stress/strain curves for ms2b, ms3b and ms5b.

Fig. 8. Damage for: from up to bottom, ms2b, ms5b (the darker, the higher the damage). Axial cuts.

strength with the increase of strain rate, and this, without requiring the use of viscosity in the model, or of any characteristic time. In other words, the increase of the dynamic strength in this range of strain rates is merely apparent and seems to be a structural effect more than a material effect as considered by the CEB formu-

lation. The next section will explore strain rate sensitivity in tension.

3.2. Dynamic tension

Initially used in compression, the SHPB technique has been extended to tension. This time, there is only one input bar, and no output bar (see Fig. 9). A projectile impacts the input bar, giving rise to a compressive wave in the input bar, which propagates into the specimen, and reflects into a tensile wave at its free end. If the wavelength of the loading pulse is longer than the specimen length, the pulse front is reflected in a tensile wave and is superposed to its own back tail still propagating. Addition of the two parts of the pulse gives rise to a tensile stress in the specimen, leading to complete rupture if its amplitude is sufficiently high. Parameters of the experiment are: acoustic impedances, sections and lengths of the projectile, of the bar, and of the specimen, as well as the impact velocity of the projectile. For a complete description, see [29].

As in compression, signals recorded by the gauges have to be separated and shifted at the impact side of the specimen.

3.2.1. The experimental data set

Tensile SHPB tests were carried out by Brara [8], Klepaczko and Brara [29] to explore higher strain rates ($20 \text{ s}^{-1} < \dot{\varepsilon} < 130 \text{ s}^{-1}$) than was available in the literature. Tested concrete has the following quasi-static characteristics: Young's modulus $E = 35$ GPa, density $\rho = 2350$ kg m^{-3}, compressive strength $\sigma_c = 42$ MPa and tensile
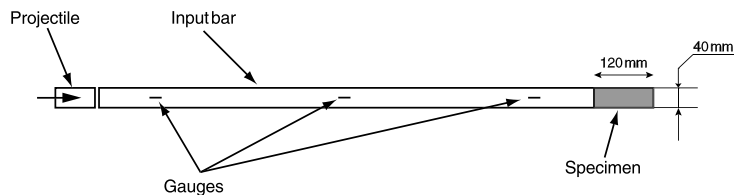

Fig. 9. Setup for SHPB experiment in tension.

9

strength $\sigma_t = 4$ MPa. Constraints listed above led to the following parameters: specimen diameter is equal to 40 mm, its length is 120 mm.

Two tests in particular were chosen, referred to here as BE16 and BE12. Table 1 shows their respective parameters. Fig. 10 shows the input forces for the two tests at the specimen face, only data available. The dynamic strength, that is to say the value of the (tensile) longitudinal stress when rupture occurs, may be evaluated in two different ways: firstly, the simulation of the propagation and superposition of the waves, and thus the determination of the stress at the known rupture position. Secondly, and more simply, ultra-high speed ccd video was used to film the tests, so it is possible to evaluate the speed of ejection of the ruptured fragment, and deduce the strength with the equation [29]

$$\sigma_{td} = \rho C_0 V_e \qquad (9)$$

where σ_{td} is the "dynamic" strength, C_0 the wave velocity, and V_e the relative velocity of the two fragments of the ruptured specimen. It is to be noted that BE16, the slowest test, led to only one rupture, while BE12, faster, led to two ruptures. In the case of multi-ruptures, the first to appear is the only one considered experimentally, in terms of critical strength, and is due to the superposition of the transmitted compressive wave and of the
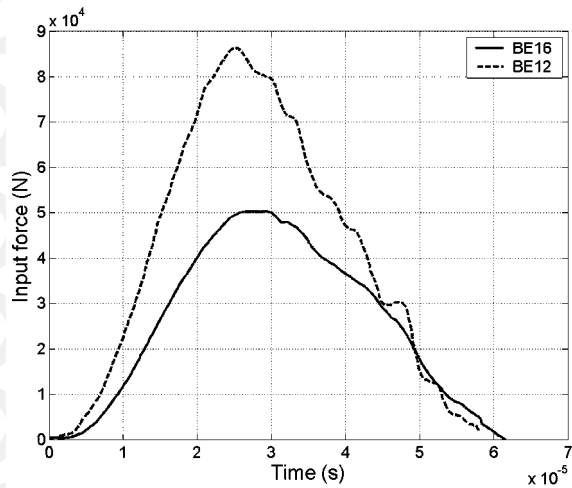
reflected tensile wave. The second rupture, occurring at quite a short distance from the first one (20/30 mm) and at nearly the same time (in roughly 10 μs), is probably due to a lot of short waves, consequence of the first rupture, which makes it difficult to explain the results concerning the second rupture.

3.2.2. The numerical setup

Numerical samples were as close to the real geometry as possible, with roughly 8000 elements, their sizes varying from 1.5 to 4 mm. Values of the local parameters were set thanks to the quasi-static procedure (see Section 2.2 or [21]) to obtain the expected macroscopic quasi-static behaviour.

Next another size distribution was used, from 1.5 to 4 mm. Experimental input forces were converted in velocity with Eq. (9), which was applied to the sample through a platen.

Results were compared with experimental ones in terms of number and position of ruptures, and of critical stress, computed through homogenization just before rupture (the chosen homogenization technique is based on an analogy with the continuous media [2,37]) and the ejection speed.

3.2.3. Results

Fig. 11 shows the state of "damage" in an axial cross-section of the specimen for both tests, with the local parameters identified in the quasi-static case. (The damage is computed per element: it is equal to the ratio number of broken interactions over the initial number of interactions. In this picture, the darker, the higher the damage). In particular, the local tensile resistance T is unchanged and is equal to 2.8 MPa, its static value. In the two tests, damage is relatively spread over the sample, and is significant: the specimen is crushed, the simulated concrete is too weak. It is to be noted that early damage occurs, even before than the compressive wave had time to reflect.

Next the local tensile resistance T was artificially increased, until the simulated results fit the experimental ones, as far as the BE16 test was concerned: T was set to 4 MPa. Fig. 12 shows the input force and the number of broken interactions (28,390 interactions are initially created) during the simulation. Table 2 compares the experimental and numerical results, obviously very close to each other.

However, with this value of $T = 4$ MPa, the BE12 test showed that the specimen is again crushed, and a uni-axial quasi-static tensile test shows a corresponding strength equal to 6.4 MPa.

Finally, the local tensile resistance T was again increased up to $T = 5.1$ MPa, so the BE12 simulation results fit the experimental ones. Fig. 13 shows the input force and the number of broken interactions during the simulation. Table 2 compares the results, again very

Table 1
Tensile test characteristics: impact velocity V_0, strain rate $\dot{\varepsilon}$, failure stress σ_{td} and rupture distance from the free end of the specimen Z_c

Test id	V_0 (m s^{-1})	$\dot{\varepsilon}$ (s^{-1})	σ_{td} (MPa)	Z_c (mm)
BE16	7.5	35.9	19.2	65.8
BE12	15	70.4	33.5	First: 69, second: 41

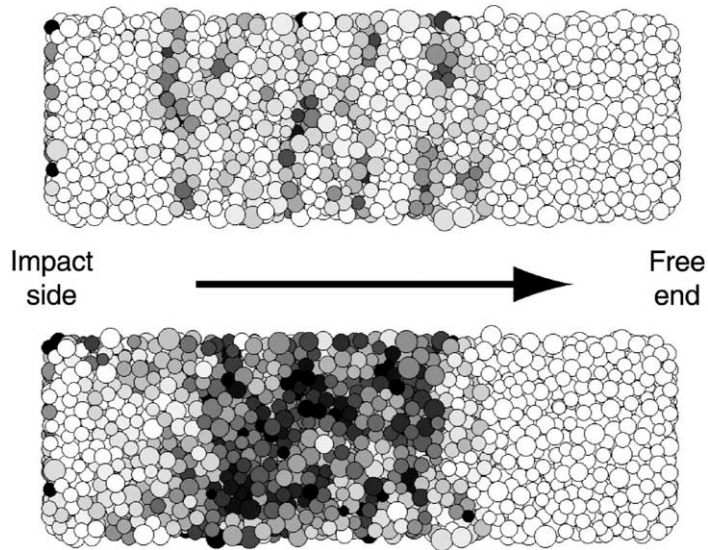Fig. 10. SHPB tension tests data set.

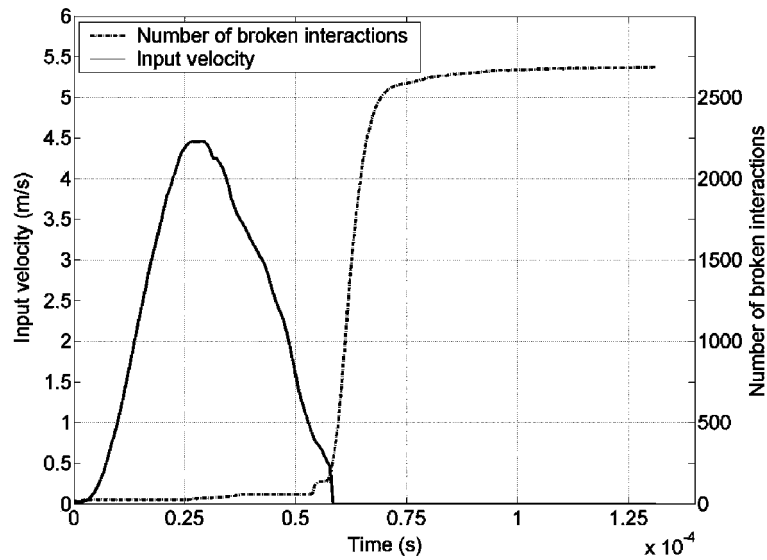Fig. 11. Damage field for: top BE16, bottom BE12.

Fig. 12. BE16 test: Input velocity and number of broken interactions versus time.

satisfactory. Homogenized stress gives a lower value than the experimental stress, which may be due to inaccurate instant of the stress computation, as both ruptures occur in less than 10 μs time. All other values seem to be correct.

If the BE16 test is simulated with this value of T, results show no rupture and only a little damage, and the corresponding quasi-static tensile strength is equal to 8.2 MPa.

3.2.4. Discussion

These results show that, unlike compressive tests, the model, unchanged, is unable to take into account strain rate dependency of concrete under tension. But on the other hand, they enable us to draw several conclusions: Firstly, inertia alone, intrinsically accounted for in the model, cannot explain strain rate dependency of concrete in tension. Secondly, the artificial increase of the local tensile resistance is enough to represent correctly

11

Table 2

Comparison between experimental and analytical results for the tensile tests: rupture distance from the free end of the specimen Z_c, failure stress σ_{td} and ejection velocity V_e

| Test id.	BE16 (with $T = 4$ MPa)	BE12 (with $T = 5.1$ MPa)	BE16 (updated model)	BE12 (updated model)
Experimental Z_c (mm)	65.8	First: 69, second: 41	65.8	First: 69, second: 41
Experimental σ_{td} (MPa)	19.2	33.5 (for the first rupture)	19.2	33.5 (for the first rupture)
Simulated Z_c (mm)	72 (at $t = 60 \times 10^{-6}$ s)	First: 75, second: 43 ($t \simeq 55 \times 10^{-6}$ s)	72 (at $t = 60 \times 10^{-6}$ s)	First: 77, second: 46 ($t \simeq 55 \times 10^{-6}$ s)
Simulated σ_{td} from homogenization (MPa)	17	23 (for both ruptures)	21	28 (for both ruptures)
Simulated V_e	2.3 (at $t = 79.1 \times 10^{-6}$ s)	First: 3.8, second: 2.2	2.4 (at $t = 81 \times 10^{-6}$ s)	First: 3.2, second: 2
Simulated σ_{td} from V_e (MPa)	20.8	First: 35, second: 20	21.7	First: 29, second: 18
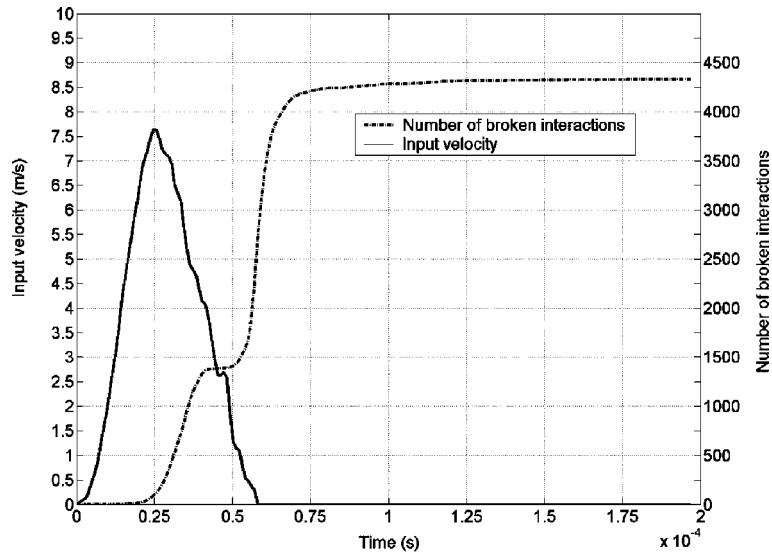
Fig. 13. BE12 test: Input velocity and number of broken interactions versus time.

the rate effect, in terms of increase of apparent tensile strength, as well as in terms of number, position and shape (nearly plane or meniscus-shaped) of ruptures. The increase of strain rate does not seem to change whatsoever the failure behaviour of concrete, everything happens like the tensile strength of concrete increases. This means that, rather than a structural effect, the strain rate dependency in tension at these strain rates seems to be a material-intrinsic behaviour. Therefore, it seems legitimate to introduce a local strain rate dependence to reproduce this behaviour. This is the purpose of the next section.

3.3. Modelling of strain rate dependence in tension

If indeed the strain rate sensitivity in tension is a material effect, the local implementation of a law of the same shape as the apparent macroscopic rate dependence should be relevant. An easy-to-use and physical relationship between the dynamic strength and the strain rate was then looked for. As at the high strain rates considered, even a dry concrete shows a rate dependence, but at a lower intensity than for a "wet" concrete [8], viscosity alone does not seem to explain the concrete dynamic behaviour. The use of a more empirical law was preferred, of the shape $\sigma_d \propto \dot{\varepsilon}^n$. It is the case of the CEB formulation which is mostly based on test results compiled from the literature, and on analytical results: Gopalaratnam et al. [19] and Klepaczko [28] deduced the same kind of law, from physical assumptions. For the sake of simplicity, it has been decided to implement a law based on the CEB formulation.

3.3.1. The CEB formulation

In tension (the formulation is different in compression), the rate dependence is given by

$$\frac{\sigma_{td}}{\sigma_{ts}} = \begin{cases} 1 & \text{for } \dot{\varepsilon} \leqslant \dot{\varepsilon}_{stat} \\ \left(\frac{\dot{\varepsilon}}{\dot{\varepsilon}_{stat}}\right)^{1.016\delta} & \text{for } \dot{\varepsilon}_{stat} < \dot{\varepsilon} \leqslant 30 \text{ s}^{-1} \\ \theta\left(\frac{\dot{\varepsilon}}{\dot{\varepsilon}_{stat}}\right)^{1/3} & \text{for } \dot{\varepsilon} > 30 \text{ s}^{-1} \end{cases} \tag{10}$$

where σ_{td} is the dynamic tensile strength at $\dot{\varepsilon}$, σ_{ts} is the static tensile strength at $\dot{\varepsilon}_{stat} = 3\times10^{-6}$, $\dot{\varepsilon}$ is the strain rate in the range of 3×10^{-6} to 300 s^{-1}, $\log(\theta) = 7.11\delta - 2.33$, $\delta = \frac{1}{10+6\frac{\sigma_{cs}}{\sigma_{co}}}$ (σ_{cs} is the compressive static strength) and $\sigma_{co} = 10$ MPa is a reference value.

Thus this formulation takes into account the following properties: The increase of strength is related to a strength measured at a specific quasi-static strain rate, it is higher for concretes with lower strengths, and in a $\log\left(\frac{\sigma_{td}}{\sigma_{ts}}\right)$ versus $\log(\dot{\varepsilon})$ plot, it is bilinear with a change of slope around 3×10^{1} s^{-1}. Nevertheless, Malvar and Crawford [34], after reviewing the properties of concrete under dynamic loading, have concluded that the CEB formulation accurately fitted the experimental results in compression, but not quite so in tension, and proposed an alternate formulation. In particular, the modified change of slope occurs at $\dot{\varepsilon} = 10^{0}$ s^{-1}, the slope of the first part δ is changed, as well as the quasi-static strain rate $\dot{\varepsilon}_{stat}$.

3.3.2. Discrete element model update and results

The model is modified so that the local tensile strength T depends on the strain rate $\dot{\varepsilon}$:

$$\frac{T_{td}}{T_{ts}} = \begin{cases} 1 & \text{for } \dot{\varepsilon} \leqslant \dot{\varepsilon}_{stat} \\ \left(\frac{\dot{\varepsilon}}{\dot{\varepsilon}_{stat}}\right)^{\delta} & \text{for } \dot{\varepsilon}_{stat} < \dot{\varepsilon} \leqslant 10^{0} \text{ s}^{-1} \\ \theta\left(\frac{\dot{\varepsilon}}{\dot{\varepsilon}_{stat}}\right)^{1/3} & \text{for } \dot{\varepsilon} > 10^{0} \text{ s}^{-1} \end{cases} \tag{11}$$

where T_{td} is the local dynamic tensile strength at $\dot{\varepsilon}$, T_{ts} is the local static tensile strength at $\dot{\varepsilon}_{stat} = 5\times10^{-6}$ s^{-1}, $\log(\theta) = \left(\frac{1}{3} - \delta\right)\log(\dot{\varepsilon}_{stat})$, and $\delta = \frac{1}{38}$, $\sigma_{co} = 10$ MPa.

Considering an interacting couple of discrete elements a and b, of velocity vectors $\mathbf{V_a}$ and $\mathbf{V_b}$, and of position vectors $\mathbf{x_a}$ and $\mathbf{x_b}$, the discrete strain rate is given by

$$\dot{\varepsilon} = \frac{(\mathbf{V_b} - \mathbf{V_a}).(\mathbf{x_b} - \mathbf{x_a})}{\|\mathbf{x_b} - \mathbf{x_a}\|^2} \tag{12}$$

Of course, attention has to be paid to the way local softening is taken into account.

In the case of the simulation of the BE16 and BE12 tests, $T_{ts} = 2.8$ MPa (identified to obtain a quasi-static tensile strength $\sigma_{ts} = 4$ MPa). Figs. 14 and 15 show the velocity field in the specimen for both tests with the modified model, at time $t = 3.28\times10^{-3}$ s after impact.

The results are compiled in Table 2, in terms of experimental failure stress, position of ruptures, and ejection velocity.

These results are very satisfying, and tend to show that the modified model is able to reproduce accurately the strain rate effect in tension: For the BE16 test, the position of the rupture is the same as in the case when the local tensile strength was artificially increased, and still very close to the experimental position. More importantly, it is also the case for the critical stress: the ejection velocity is nearly unchanged, and the homogenized stress is even more accurate. For the BE12 test, the positions of ruptures are again close to
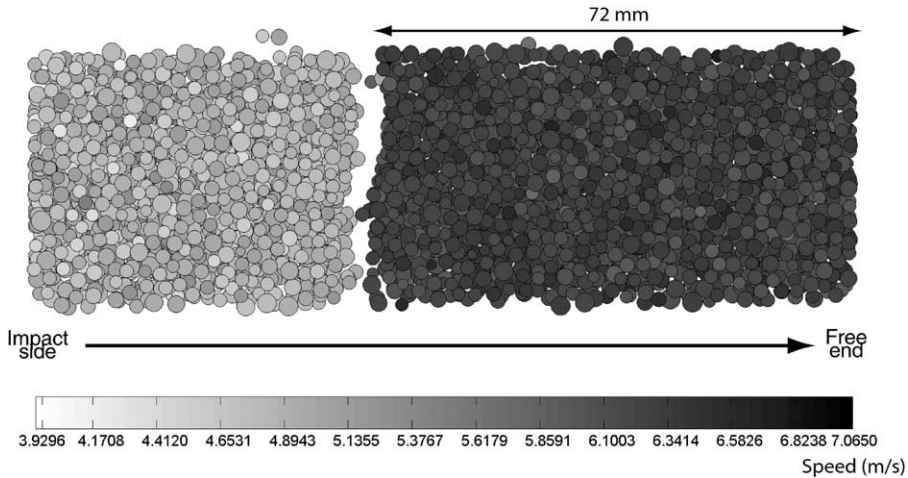

3.9296 4.1708 4.4120 4.6531 4.8943 5.1355 5.3767 5.6179 5.8591 6.1003 6.3414 6.5826 6.8238 7.0650

Speed (m/s)

Fig. 14. BE16 test with the modified model: Axial speed field in the specimen at $t = 3.28\times10^{-3}$ s.
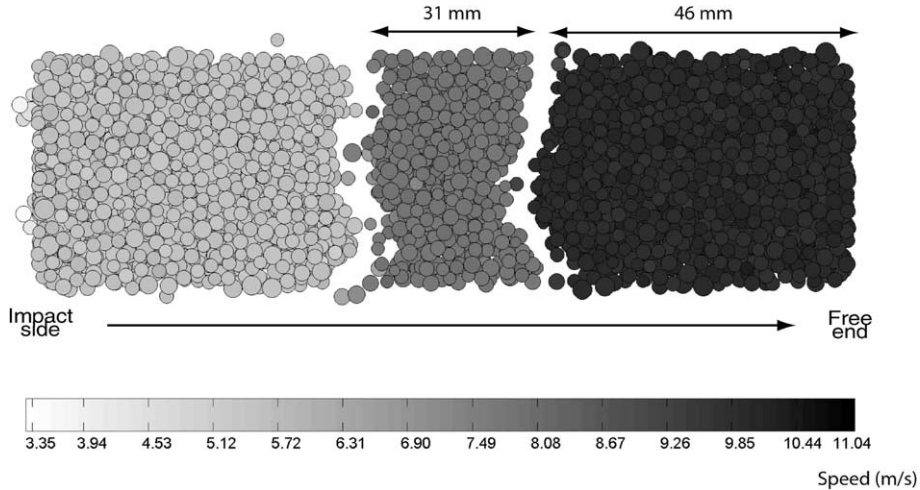
13

Fig. 15. BE12 test with the modified model: Axial speed field in the specimen at $t = 3.28 \times 10^{-3}$ s.

the experimental ones. The critical stresses, slightly lower than the experimental result, are very close to each other, whether deduced from homogenization or from the ejection velocity, at least as far as the first rupture is concerned.

4. Conclusion

In previous work, a three-dimensional discrete element approach was proposed to study the dynamic behaviour of concrete. The main specificities of this approach are the following: the modelling scale is higher than the heterogenity scale, so the model may be used in the future to simulate real structures, which means the DEM is used here only for its ability to treat discontinuities; the introduced interaction laws are then very simple and are close to macroscopic laws; last, an identification process based on quasi-static tests is used, so the quasi-static behaviour of concrete is reproduced.

The present work aims at further validating this approach through dynamic tests, and at investigating concrete behaviour. The parameters are calibrated with the quasi-static procedure, which means that the computations here are really predictive.

First compressive SHPB tests were simulated, at strain rates ranging from 350 to 700 s^{-1}. Real properties of the considered concrete are obtained through the quasi-static calibration of the local parameters. Thanks to this step, the results of the simulation of the dynamic tests are very satisfying, qualitatively, as well as quantitatively, despite the great difficulty involved in reproducing such tests. The concrete apparent strain rate sensitivity is well represented, and this, without requiring the use of any viscosity or characteristic time in

the model. The discrete element method allows the investigation of the transient phenomena (stresses, damage) in the specimen, during and after impact. This confirmed the inertia-based hypothesis: In this range of strain rates, the increase of load-carrying capacity of concrete comes from the transition from a state of uniaxial strain to a state of uniaxial stress, associated with bulking; it is a structure effect.

Then simulations of tensile SHPB tests were run, at strain rates ranging from 36 to 70 s^{-1}. Unchanged, the model did not show any strain rate dependency, but an increase of the local tensile strength is enough to fit the experimental results. This finding tends to show firstly that inertia alone cannot explain the increase of strength in this range of strain rates, and secondly that in tension, the rate sensitivity is more a material intrinsic effect. This justifies the introduction of a local discrete rate dependence law. The pattern, the number and the positions of the ruptures are accurately simulated, as well as the increase of strength.

These simulations have extended the validation of the method to model concrete under these types of loading. Another step before real concrete structures under impact could be modelled, is the validation of the model through the simulation of beam-bending tests, and the introduction of the reinforcement. This will show whether the model is able to exhibit good results in different configurations, in terms of both loading and size of the structure.

References

[1] 1993 CEB-FIP model code 1990. Comité Euro-international du Béton. Trow-bridge, Wiltshire, UK: Redwood books.

14

[2] Bardet J-P. Introduction to computational granular mechanics. In: Actes Du Collogue CISM, Udine, 1997.

[3] Bazant ZP, Oh BH. Crack-band theory for fracture of concrete. Mater Struct 1983;16:155–77.

[4] Bischoff PH, Perry SH. Compressive behaviour of concrete at high strain rates. Mater Struct 1991;24:425–50.

[5] Bischoff PH, Perry SH. Impact behavior of plain concrete loaded in uniaxial compression. J Eng Mech 1995;121(6): 685–93.

[6] De Borst R, Sluys LJ. Localization in a Cosserat continuum under static and dynamic loading conditions. Comp Methods Appl Mech Eng 1990;90:805–27.

[7] Brace WF, Jones AH. Comparison of uniaxial deformation in shock and static loading of three rocks. J Geophys Res 1971;76:4913–21.

[8] Brara A. Etude expérimentale de la traction dynamique du béton par écaillage. PhD thesis. Université de Metz, 1999 (in French).

[9] Calvetti F, Viggiani G, Tamagnini C. A numerical investigation of the incremental non-linearity of granular soils. Ital Geotech J 2003;3(3):11–29.

[10] Camborde F, Mariotti FC, Donzé F-V. Numerical study of rock and concrete behaviour by discrete element modelling. Comput Geotech 2000;27(4):225–47.

[11] Cundall PA. Numerical experiments on localization in frictional materials. Ingenieur-archiv 1989;59: 148–59.

[12] Cundall PA, Strack ODL. A discrete numerical model for granular assemblies. Géotechnique 1979;29(1):47–65.

[13] Donzé F-V. SDEC (Spherical Discrete Element Code), Version 2.00, isrn geonum-nst-2001-03-fr edn, France, 2001. Available from <www.geonum.com>.

[14] Donzé F-V. Packing spherical discrete elements of unequal size. Tech. Rep. ISRN: GEONUM-NST-2002-02-FR+ ENG. GEONUM Report, 2002, France. Available <www.geonum.com>.

[15] Ehlers W, Diebels S, Michelitsch T. Microscopic modelling of granular materials taking into account particle rotations. Lect Note Phys 2001;568:259–74.

[16] Gary G. Essais à grande vitesse sur béton. Problèmes spécifiques. Tech. Rep. GRECO, Paris, 1990 (in French).

[17] Gary G, Bailly P. Behaviour of quasi-brittle material at high strain rate, experiment and modelling. Eur J Mech, A/ Solids 1998;17(3):403–20.

[18] Gary G, Zhao H. Measurements of the dynamic behaviour of concrete under impact loading. In: Proceedings of 2nd ISIE'96, Beijing, China, 1996.

[19] Gopalaratnam V, Gerstle W, Isenberg J, Mindess S, 1996. State-of-the-art report on dynamic fracture. ACI Committee 446.

[20] Hentz S, Daudeville L, Donzé F-V. Identification of the constitutive behavior of concrete through quasi-static discrete element simulations. In: Ling HI, Anandarajah A, Manzari MT, Kaliakin VN, Smyth A, editors. Constitutive modeling of geomaterials. Boca Raton, FL, USA: CRC Press; 2003. p. 113–21.

[21] Hentz S, Daudeville L, Donzé F-V. Identification and validation of a discrete element model for concrete. J Eng Mech, ASCE 2004;130 (6 (1)).

[22] Hild F, Brajer X, Denoual C, Forquin P. On the probabilistic–deterministic transition involved in a fragmentation process of brittle materials. Comput Struct 2003;81:1241–53.

[23] Huang H. Discrete element modeling of tool-rock interaction. PhD thesis. University of Minnesota, 1999.

[24] Iwashita K, Oda M. Micro-deformation mechanism of shear banding process based on modified distinct element method. Powder Technol 2000;109:192–205.

[25] Janach W. The role of bulking in brittle failure of rocks under rapid compression. Inter J Rock Mech Min Sci Geomech Abstr 1976;13:177–86.

[26] Jodrey WS, Tory EM. Computer simulation of close random packing of equal spheres. Phys Rev A 1985;32(4): 2347–51.

[27] Johnson S, Williams J. Formation of packing structures in discrete element modeling with disks. In: 3rd Int. Conf. Proceedings on Discrete Element Methods. Sandia Laboratories, Santa Fe, NM, 2002.

[28] Klepaczko JR. Dynamic crack initiation. Some experimental methods and modelling. Vienna: Springer-Verlag; 1990.

[29] Klepaczko JR, Brara A. An experimental method for dynamic tensile testing of concrete by spalling. Int J Impact Eng 2001;25:387–409.

[30] Kuhn MR, Bagi K. Particle rotations in granular materials. In: 15th ASCE Engineering Mechanics Conference. ASCE, Columbia University, New York, NY, 2002.

[31] Kusano N, Aoyagi T, Aizawa J, Ueno H, Morikawa H, Kobayashi N. Impulsive local damage analyses of concrete structure by the distinct element method. Nucl Eng Des 1992;138:105–10.

[32] Liao C-L, Chang T-R, Young D-H, Chang CS. Stress-strain relationship for granular materials based on the hypothesis of best fit. Int J Solids Struct 1997;34(31–32): 4087–100.

[33] Lilliu G, Van Mier JGM. 3d lattice type fracture model for concrete. Eng Fract Mech 2003;70:927–41.

[34] Malvar LJ, Crawford JE. Dynamic increase factors for concrete. In: 28th Department of Defense Explosives Safety Seminar, Orlando, FL, 1998.

[35] Mazars J. Application de la mécanique de l'endommagement au comportement non linéaire et à la rupture du béton de structure. PhD thesis. thèse de doctorat d'état de l'université Paris VI, 1984 (in French).

[36] Meguro K, Hakuno M. Fracture analyses of concrete structures by the modified distinct element method. Structural Eng/Earthquake Eng 1989;6(2):283–94.

[37] Moreau J-J. Numerical investigation of shear zones in granular materials. In: Grassberger P, Wolfs D, editors. Friction, arching, contact dynamics. Singapore: World Scientific Editions; 1997. p. 233–47.

[38] Pijaudier-Cabot G, Benallal A. Strain localization and bifurcation in a nonlocal continuum. Int J Solids Struct 1993;30(13):1761–75.

[39] Potapov AA, Hopkins MA, Campbell CS. A two-dimensional dynamic simulation of solid fracture. Part I: Description of the model. Int J Modern Phys 1995;6(3): 371–98.

[40] Potyondi D, Cundall PA, 1999. Modeling notch formation in the URL mine-by tunnel: Phase IV—enhancements to the PFC model of rock. Tech. Rep. 06819-REP-01200-10002-R00. Itasca consulting group Inc.

[41] Potyondy DO, Cundall PA, Lee CA. Modelling rock using bonded assemblies of circular particles. Rock Mech 1996:1937–44.

[42] Rossi P, Van Mier JGM, Toutlemonde R, Le Maou F, Boulay C. Effect of loading rate on the strength of concrete subjected to uniaxial tension. Mater Struct 1994;27: 260–4.

[43] Thabet A, Haldane D. Three-dimensional numerical simulation of the behaviour of standard concrete test specimens when subjected to impact loading. Comput Struct 2001;79:21–31.

[44] Toutlemonde F. Résistance au choc des structures en béton; du comportement du matériau au calcul des ouvrages. PhD thesis. Ecole Nationale des Ponts et Chaussées, 1995 (in French).

[45] Toutlemonde F, Rossi P. Major parameters governing concrete dynamic behaviour and dynamic failure of concrete structures. In: Euro-DYMAT94, GB: Oxford; 1994. p. 26–30.

[46] Zhao H, Gary G. On the use of SHPB techniques to determine the dynamic behavior of materials in the range of small strains. Int J Solids Struct 1996;33(23):3363–75.